Chapter-VI

X-Ray Diffraction
&
Inductively Coupled Plasma Mass Spectroscopy (ICPMS)

6.1 Introduction

In many geologic investigations, XRD complements other mineralogical methods, including optical light microscopy, electron microprobe microscopy (EMM), and scanning electron microscopy (SEM). X-ray diffraction is a versatile, non-destructive analytical technique for identification and quantitative determination of the various crystalline compounds, known as 'phases', present in solid materials and powders. It provides the researcher with a fast and reliable tool for routine mineral identification. It is particularly useful for identifying fine-grained minerals and mixtures or intergrowths of minerals, which may not lend themselves to analysis by other techniques.

XRD can provide additional information beyond basic identification like degree of crystallinity of the mineral (s) present; possible deviations of the minerals from their ideal compositions (presence of element substitutions and solid solutions); the structural state of the minerals (which can be used to deduce temperatures and (or) pressures of formation); and the degree of hydration for minerals that contain water in their structure. Some mineralogical samples analyzed by XRD are too fine grained to be identified by optical light microscopy.

The three-dimensional structure of nonamorphous materials, such as minerals, is defined by regular, repeating planes of atoms that form a crystal lattice. When a focused X-ray beam interacts with these planes of atoms, part of the beam is transmitted, part is absorbed by the sample, part is refracted and scattered, and part is diffracted. Diffraction of an X-ray beam by a crystalline solid is analogous to diffraction of light by droplets of water,

producing the familiar rainbow. X-rays are diffracted by each mineral differently, depending on what atoms make up the crystal lattice and how these atoms are arranged.

A crystal lattice is a regular three-dimensional distribution (cubic, rhombic, etc.) of atoms in space. These are arranged so that they form a series of parallel planes separated from one another by a distance d, which varies according to the nature of the material. For any crystal, planes exist in a number of different orientations- each with its own specific d-spacing. When illuminated by an X-ray source, crystalline material will generate X-ray diffraction peaks. The peak positions are described by the crystal unit cell parameters, and the peak intensities are given by the placement of the atoms in the unit cell. The peak widths are a result of two parameters, finite crystallite sizes and micro-stress within the crystallites. As such, the parameters that define a different crystal structure can be simply accessed from an X-ray diffraction patterns. Each mineral type is defined by a characteristic crystal structure, which will give a unique X-ray diffraction pattern, allowing rapid identification of minerals present within rock or soil sample.

Identification is achieved by comparing the X-ray diffraction pattern - or 'diffractogram' - obtained from an unknown sample with an internationally recognised database containing reference patterns for more than 70,000 phases.

Modern computer-controlled Defractometer systems use automatic routines to measure, record and interpret the unique diffractogram produced by individual constituents in even highly complex mixtures.

6.2 X-Ray powder diffraction of beach sediments of the study

Beach sediments, composed of minerals may be studied by various analytical techniques. One such technique, X-ray powder diffraction (XRD), is an instrumental technique that is used to identify minerals, as well as other crystalline materials.

In the present study of beach sediments from the east coast of India XRD patterns have been done for samples collected from six beaches namely, Puri, Gopalpur, Kalingapatnam, Vishakhapatnam, Kakinada, and Vedaranniyam (Map 1.1). The analyses were performed at the Laboratory of Tata Refractories Limited, Belpahar, District Jharsugoda (Orissa) with the help of X-ray Defractometer (Phillips Holland- Model TW 1730 S 1970).

The analysis has been carried to confirm some of the heavy minerals in support of the identification done in thin sections. To do so D-Spacing chart for Cobalt Target have been prepared. These charts give peak-values corresponding to the minerals in all the selected stations.

6.2.1 Puri beach

The **Graph I** represents the sample of Puri Beach and reveals D-values of zircon (3.30, 4.43, 2.52), verities of garnet like spessartite (2.60, 1.58, 2.96), grossularite (2.65, 1.58, 2.96) and garnet-pyrope (2.89, 2.58, 1.54), tourmaline (2.58, 3.99, 2.96), magnetite (2.53, 1.49, 2.97), ilmenite (2.74, 1.72, 2.54), rutile (3.25, 1.69, 2.49), hornblende (2.55, 1.44, 2.68), monazite (3.09, 2.87, 3.30), sphene (3.23, 1.64, 1.49) and andalusite (5.58, 2.79, 3.96) minerals. While the later shows those of epidote (2.90, 2.68, 2.69), staurolite (3.01, 2.69, 2.37) and anatase (3.51, 1.89, 2.38), as shown in **Plate 1-2**.

Graph I : XRD pattern of sample Puri

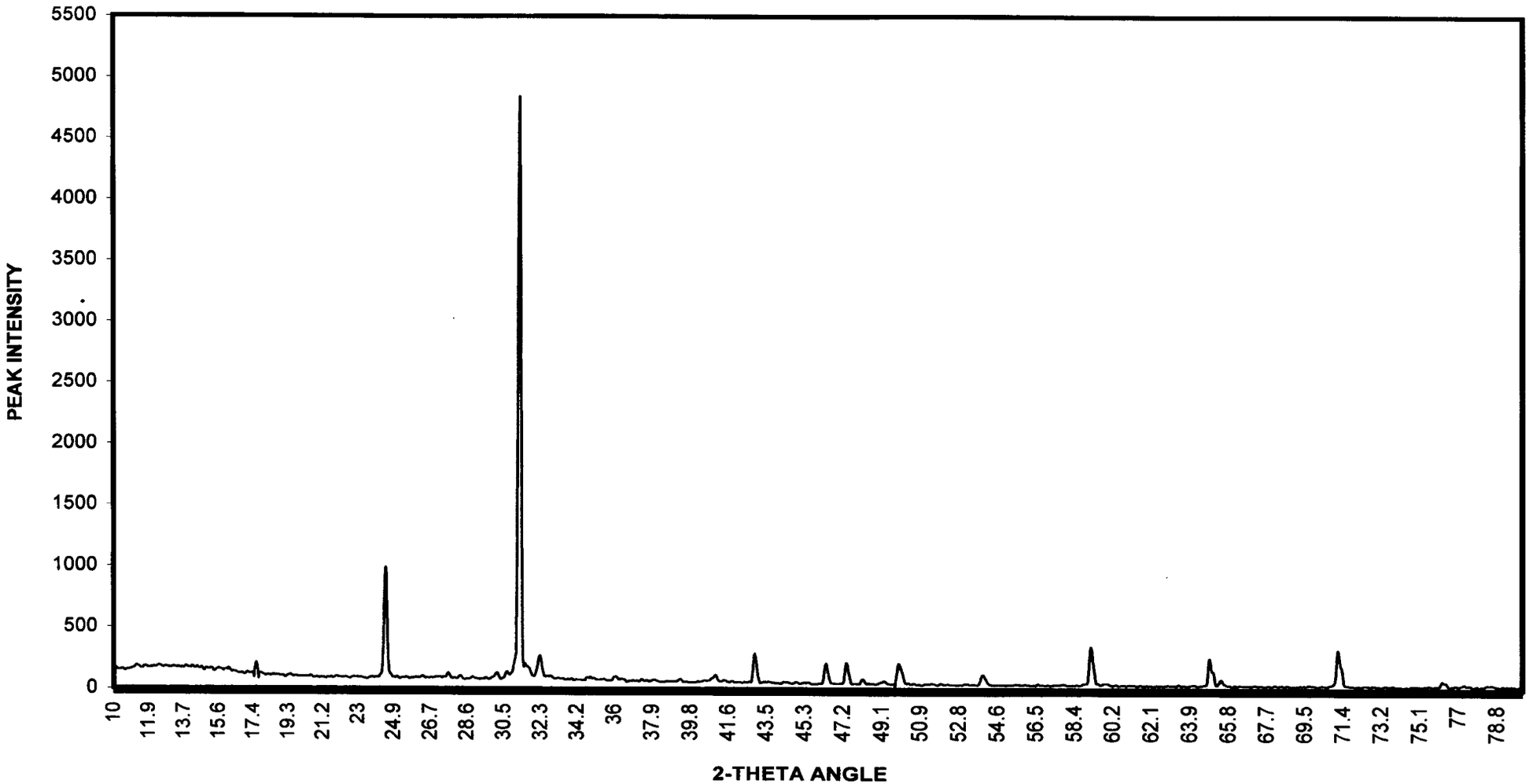

124

6.2.2 Gopalpur beach

Graph II of Gopalpur beach shows abundance of kyanite (3.18, 1.37, 1.93), biotite (10.10, 3.37, 2.66), augite(2.99, 1.62, 1.43), zircon (3.30, 4.43, 2.52), verities of garnet like spessartite (2.60, 1.58, 2.96) and grossularite (2.65, 1.58, 2.96); tourmaline (2.58, 3.99, 2.96); magnetite (2.53, 1.49, 2.97); ilmenite (2.74, 1.72, 2.54); rutile (3.25, 1.69, 2.49); hornblende (2.55, 1.44, 2.68); monazite (3.09, 2.87, 3.30); andalusite (5.58, 2.79, 3.96) minerals. While the later shows those of epidote (2.90, 2.68, 2.69) and staurolite (3.01, 2.69, 2.37), as shown in **Plate 3**.

6.2.3 Kalingapatnam beach

Graph III of Kalingapatnam beach sediments reveals the presence of sillimanite (3.36, 2.20, 3.40); zircon (3.30, 4.43, 2.52); verities of garnet like spessartite (2.60, 1.58, 2.96) and grossularite (2.65, 1.58, 2.96); tourmaline (2.58, 3.99, 2.96); magnetite (2.53, 1.49, 2.97); ilmenite (2.74, 1.72, 2.54), rutile (3.25, 1.69, 2.49); hornblende (2.55, 1.44, 2.68); monazite (3.09, 2.87, 3.30); sphene (3.23, 1.64, 1.49); and andalusite (5.58, 2.79, 3.96). While the later shows those of epidote (2.90, 2.68, 2.69), staurolite (3.01, 2.69, 2.37), anatase (3.51, 1.89, 2.38) and magnetite as prominent heavies, as shown in **Plate 4**.

Graph II : XRD pattern of sample Gopalpur

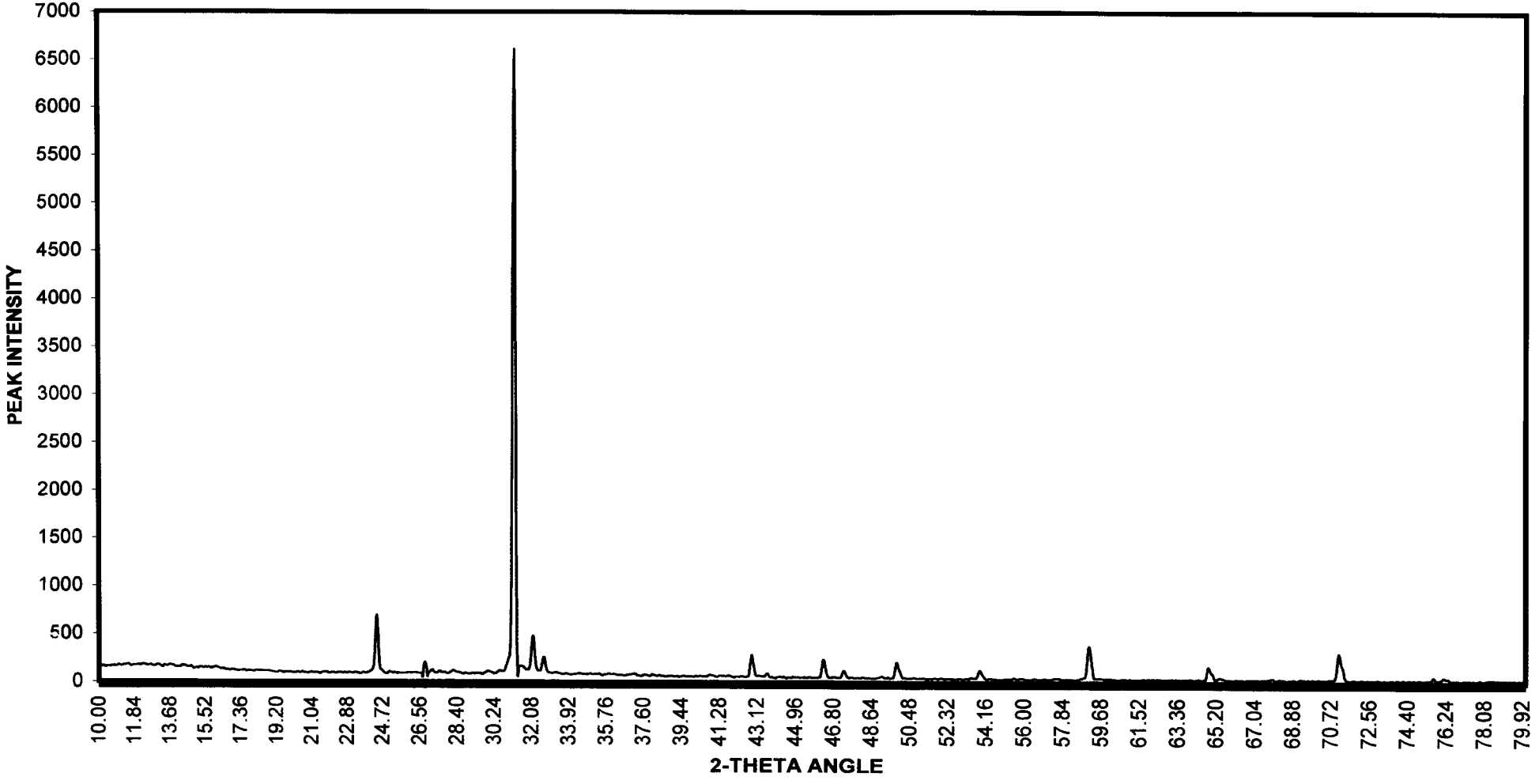

Graph III : XRD pattern of sample Kalingapatnam

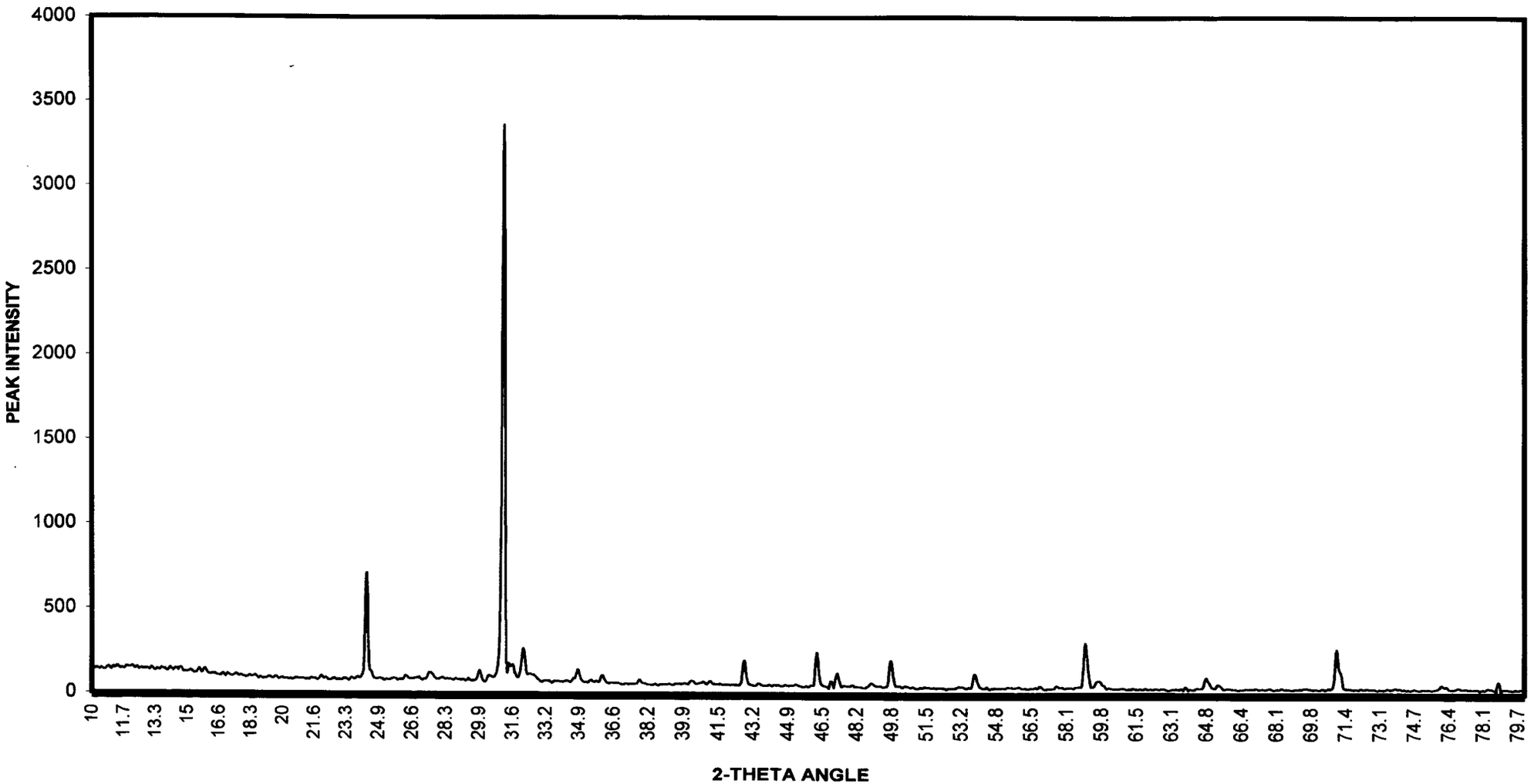

6.2.4 Vishakhapatnam beach

Graph IV from Vishakhapatnam beach strongly denotes zircon (3.30, 4.43, 2.52), verities of garnet like spessartite (2.60, 1.58, 2.96) and grossularite (2.65, 1.58, 2.96); tourmaline (2.58, 3.99, 2.96); magnetite (2.53, 1.49, 2.97); ilmenite (2.74, 1.72, 2.54); rutile (3.25, 1.69, 2.49); hornblende (2.55, 1.44, 2.68); monazite (3.09, 2.87, 3.30) and andalusite (5.58, 2.79, 3.96). While the later shows epidote (2.90, 2.68, 2.69), staurolite (3.01, 2.69, 2.37) and anatase (3.51, 1.89, 2.38) (**Plate 5**).

6.2.5 Kakinada beach

Graph V represents peak value of Kakinada beach sediments where abundant of zircon (3.30, 4.43, 2.52), verities of garnet like spessartite (2.60, 1.58, 2.96) and grossularite (2.65, 1.58, 2.96); tourmaline (2.58, 3.99, 2.96); magnetite (2.53, 1.49, 2.97); ilmenite (2.74, 1.72, 2.54); rutile (3.25, 1.69, 2.49); hornblende (2.55, 1.44, 2.68); sphene (3.23, 1.64, 1.49); and andalusite (5.58, 2.79, 3.96). While the later shows those of epidote (2.90, 2.68, 2.69); staurolite (3.01, 2.69, 2.37); anatase (3.51, 1.89, 2.38); olivine (2.73, 1.91, 3.01) and diopside (2.99, 2.52, 2.89), as shown in **Plate 6**.

6.2.6 Vedaranniyam beach

Graph VI represents Vedaranniyam beach shows the abundance of zircon (3.30, 4.43, 2.52), verities of garnet like spessartite (2.60, 1.58, 2.96) and grossularite (2.65, 1.58, 2.96); tourmaline (2.58, 3.99, 2.96); magnetite (2.53, 1.49, 2.97); ilmenite (2.74, 1.72, 2.54); rutile (3.25, 1.69, 2.49); horn-

Graph IV : XRD Pattern of sample Vishakhapatnam

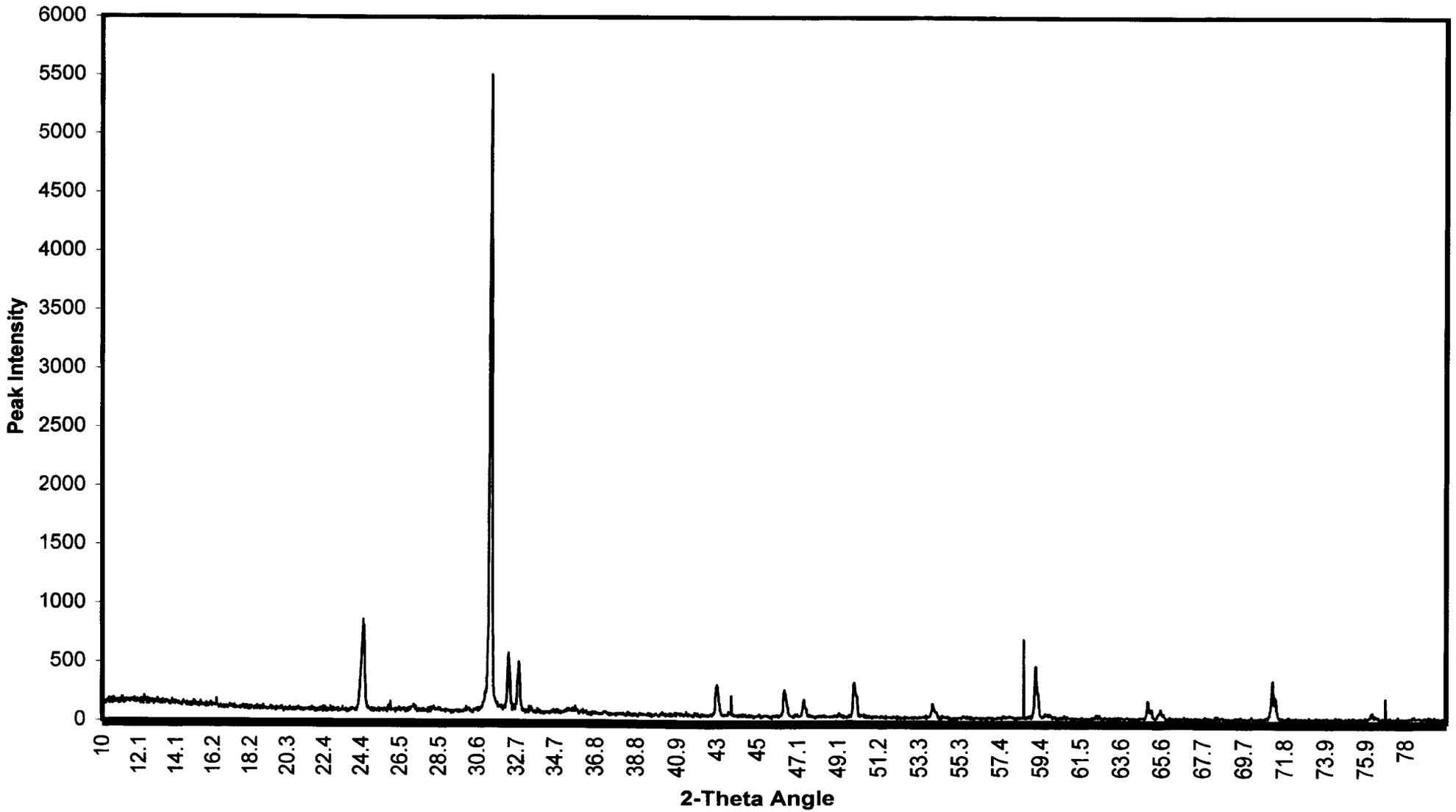

Graph V : XRD pattern of sample Kakinada

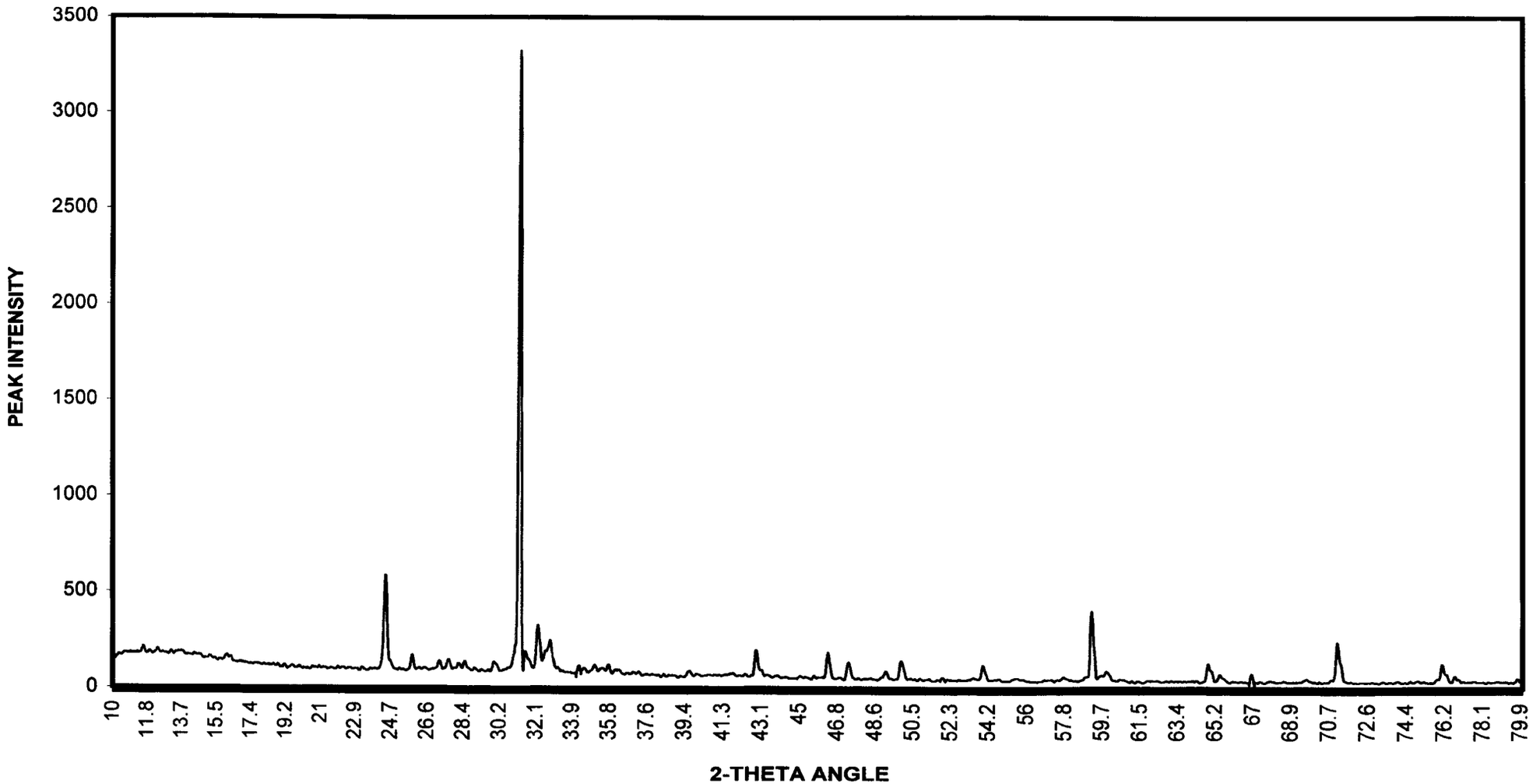

Graph VI : XRD Pattern of Sample Vedaranniyam

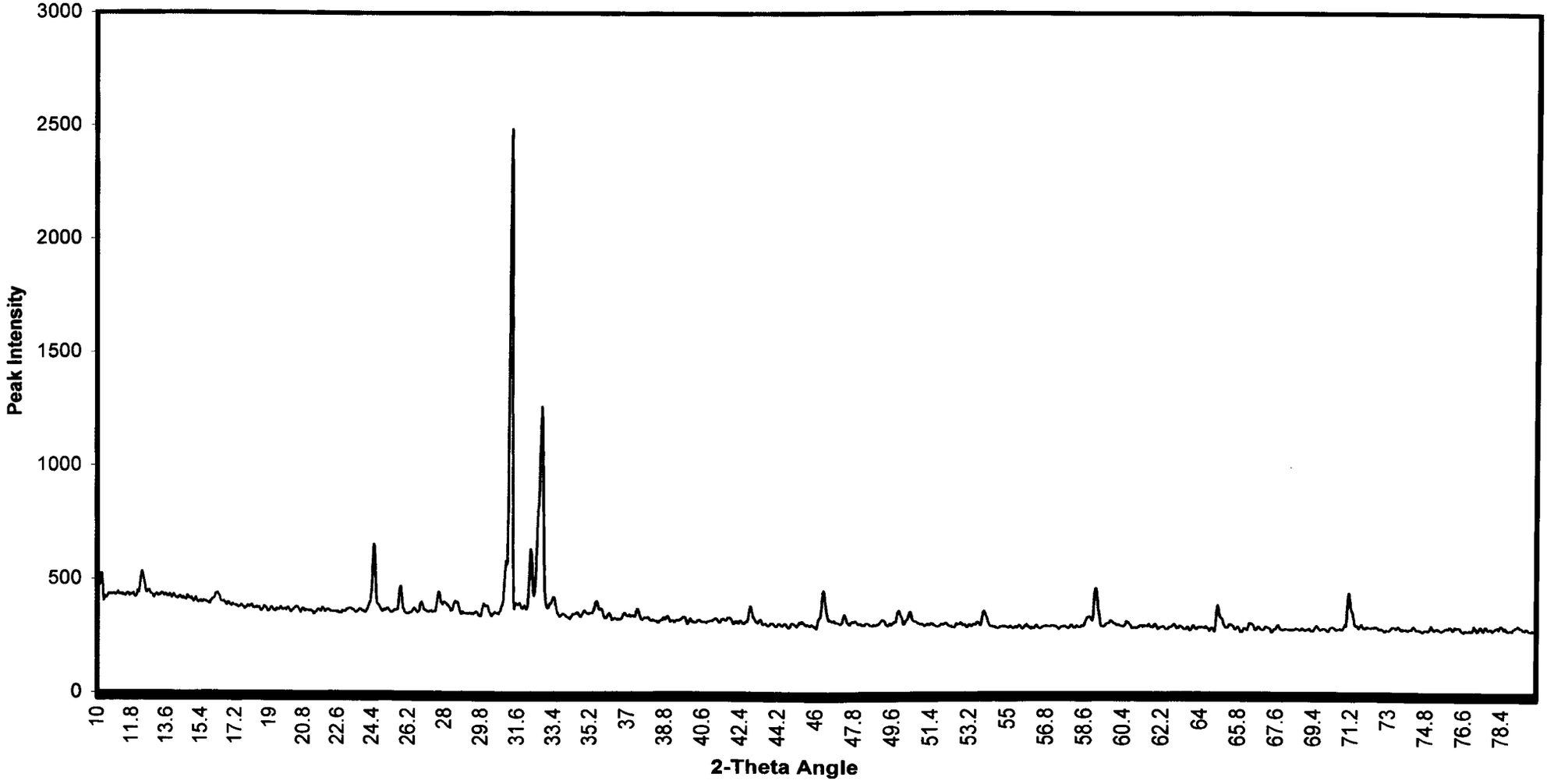

blende (2.55, 1.44, 2.68); sphene (3.23, 1.64, 1.49); and andalusite (5.58, 2.79, 3.96). While the later shows epidote (2.90, 2.68, 2.69); anatase (3.51, 1.89, 2.38); spinel (2.44, 2.02, 1.43); and sillimanite (3.36, 2.20, 3.40). The most striking feature of this graph is the presence of peak values of diamond (2.01, 1.26, 1.08) which attests the result of mounted grain study of the material from the Vedaranniyam beach as shown in **Plate 11.**

The results of the present XRD analyses from the selected beach samples confirm the identification of the heavy minerals studied microscopically.

6. 3 Inductively coupled plasma mass spectroscopy (ICP-MS)

6.3.1 Introduction

ICP-MS analysis is one of the most powerful methods for the quantitative determination of trace and ultra-trace elements in sub ppm levels. The advantage of the method is its high sensitivity and the simple spectra of the elements to avoid 'concentration of the target elements by ion exchange'.

The ICP-MS analyses of samples Stations (Map 1.1) namely, Puri, Gopalpur, Kalingapatinam, Vishakhapatnam, Kakinada, Chirala, Chennai, Nagapattinam, Vedaranniyam, Kottipattinam, Rameshwarm, Kanniyakumari have been carried by Prof. T. Ishiyama in the ICPMS laboratory at the Institute of Applied Earth Sciences, Akita University, Akita, Japan in 1999.

6.3.2 Methodology: Open Acid Digestion (OAD)

The ordinal ICP-MS system requires solution samples because the samples are nebulized for introduction of aroma-plasma. The Open Acid Digestion (OAD) (Kimura *et al.,* 1995) has been employed in the present analysis. The sediments of the selected beaches were first powdered and then decomposed using acid digestion. Samples of 0.5gm were weighed accurately by electric balance. Each sample was then put in to beakers (PTFF) and 5ml of 45% HF was added to it. The mixture of powders and acids were kept at 100°C for an hour. The temperature was then increased to 200°C gradually, and samples were evaporated to dryness. The $HCLO_4$ + HF digestion process was replicated once more, and then cooled down. Ten ml of 60% HNO_3 and 30ml of di-ionized water were added into PTEE beakers and boiled gently for three hours. After cooling down, the sample solutions were diluted to 100ml in volumetric flasks by adding di-ionized water. The dilution factor becomes 200 times. These samples were kept in polyethylene bottles.

Computation

The Inductively Coupled Plasma Mass Spectroscopy (ICP-MS) for trace and ultra-trace elements including Rare Earth Elements (REE) of samples from eight stations reveals distribution of Manganese (Mn), Gallium (Ga), Rubidium (Rb), Strontium (Sr), Yttrium (Y), Niobium (Nb), Tin (Sn), Antimony (sb), Caesium (Cs), Barium (Ba), Lanthanum (La), Cerium (Ce), Praseodymium (Pr), Neodymium (Nd), Samarium (Sm), Europium (Eu),

Gadolinium (Gd), Terbium (Tb), Dysprosium (Dy), Holmium (Ho), Erbium (Er), Thulium (Tm), Ytterbium (Yb), Lutetium (Lu), Hafnium (Hf), Thorium (Th), and Uranium (U).

Most of the Chondrite-normalized REE patterns show metamorphic and igneous affinities as shown in Table 6.1.

The study also shows higher values (all in ppm) of Pr (100), Sm and Tm (80 each), U and Hf (10 each) at Puri; Ba (over 1000), Rb, Sr, Ce (100 each), Nd and Th (45 each) at Kalingapatinam; Ba (1000), Rb and Sr (100), Th (8) and La, Ce, Nd Sm, Gd and Hf, (around 6 each) at Vishakhapatnam; Sr (500) and Rb (100), Th (8) at Kakinada; Ba (7000), Sr and Rb (around 1000 each), La and Ce (around 80 each), Nd and Th around 50 each) and U (7) at Chirala; Sr, Ba, La and Ce around (1000 each), Nd and Th (around 100 each); Sr (8000), Ba (600) at Vedaranniyam; and Ba (5000), Sr (100) at Tondi beaches.

Table 6.1 Provenances based ICPMS & dominance of igneous and metamorphic minerals

S. No.	Beach	Provenance Based on ICPMS	Igneous/ Metamorphic Minerals
1	Puri	Igneous	Igneous
2	Gopalpur	Metamorphic	Metamorphic
3	Kalingapatnam	Metamorphic	Metamorphic
4	Vishakhapatnam	Metamorphic	Metamorphic
5	Kakinada	Metamorphic	Metamorphic
6	Chirala	Metamorphic	Metamorphic
7	Chennai	Igneous, Meta (?)	Metamorphic
8	Nagapattinam	Igneous	Metamorphic
9	Vedaranniyam	Metamorphic	Metamorphic
10	Kottipattinam	Metamorphic	Metamorphic
11	Tondi	Metamorphic	Metamorphic
12	Mandapam	Metamorphic	Metamorphic
13	Rameshwarm	Metamorphic	Metamorphic
14	Tuticorin	Metamorphic	Metamorphic
15	Kanniyakumari-II	Igneous	Metamorphic

Fig 6.2 A: ICP-MS analysis

(Ga, Rb, Sr, Y, Cs, Ba, La, Ce, Pr, Nd, Sm, Eu, Gd, Tb, Dy, Ho, Er, Tm, Yb, Lu, Hf, Th, U)

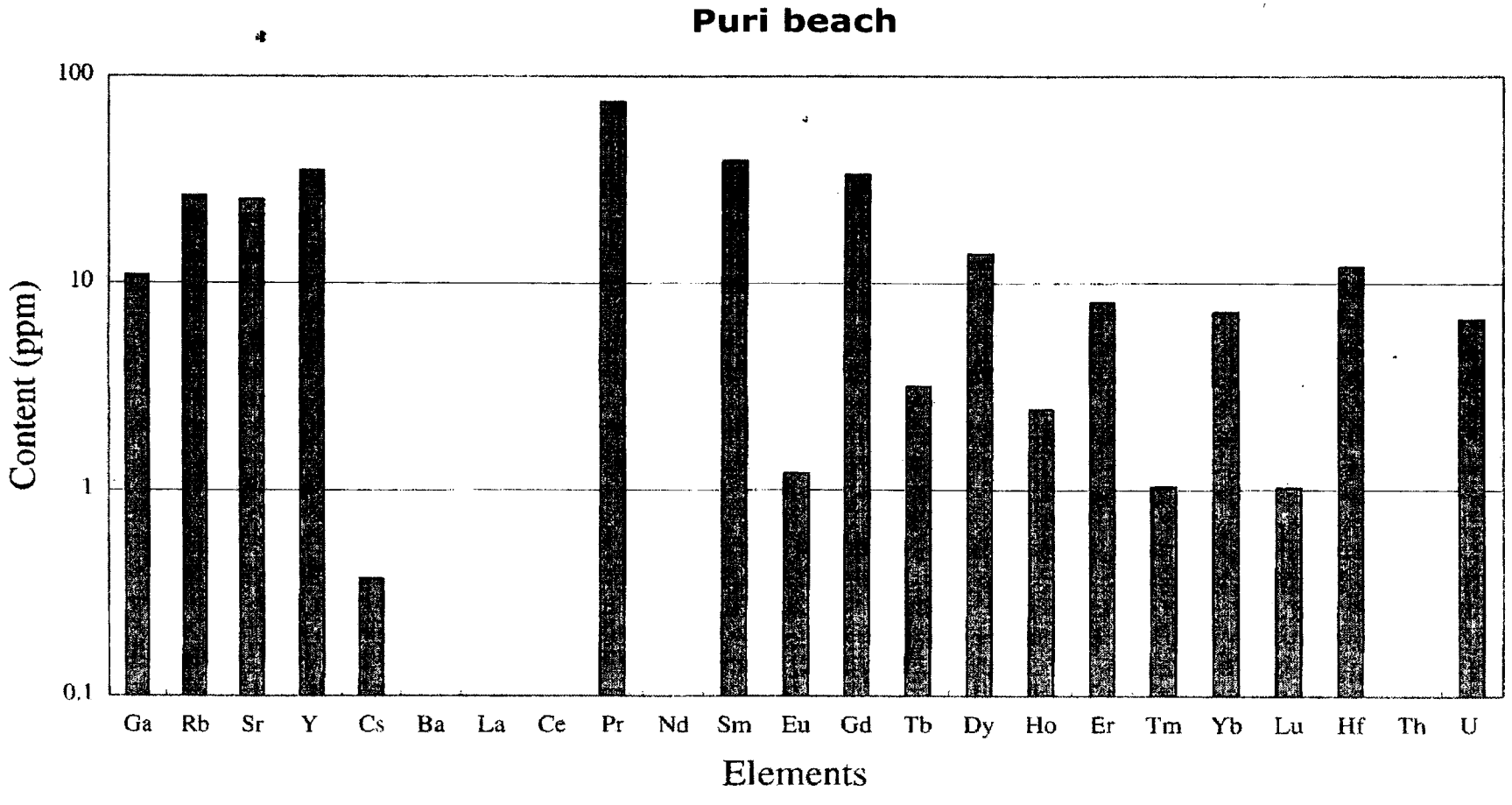

Fig 6.2 B: ICP-MS analysis

(Ga, Rb, Sr, Y, Cs, Ba, La, Ce, Pr, Nd, Sm, Eu, Gd, Tb, Dy, Ho, Er, Tm, Yb, Lu, Hf, Th, U)

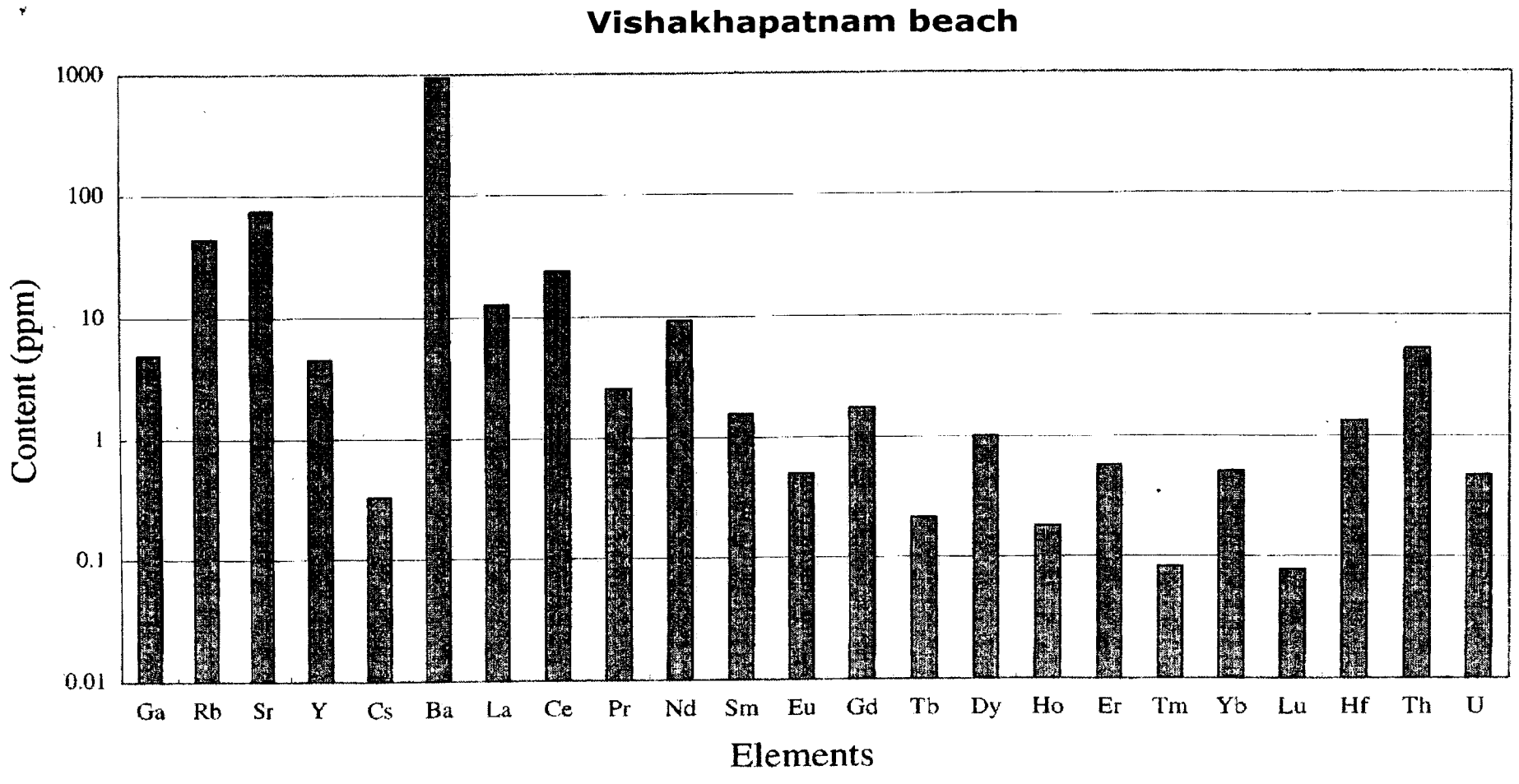

Fig 6.2 C: ICP-MS analysis
(Ga, Rb, Sr, Y, Cs, Ba, La, Ce, Pr, Nd, Sm, Eu, Gd, Tb, Dy, Ho, Er, Tm, Yb, Lu, Hf, Th, U)

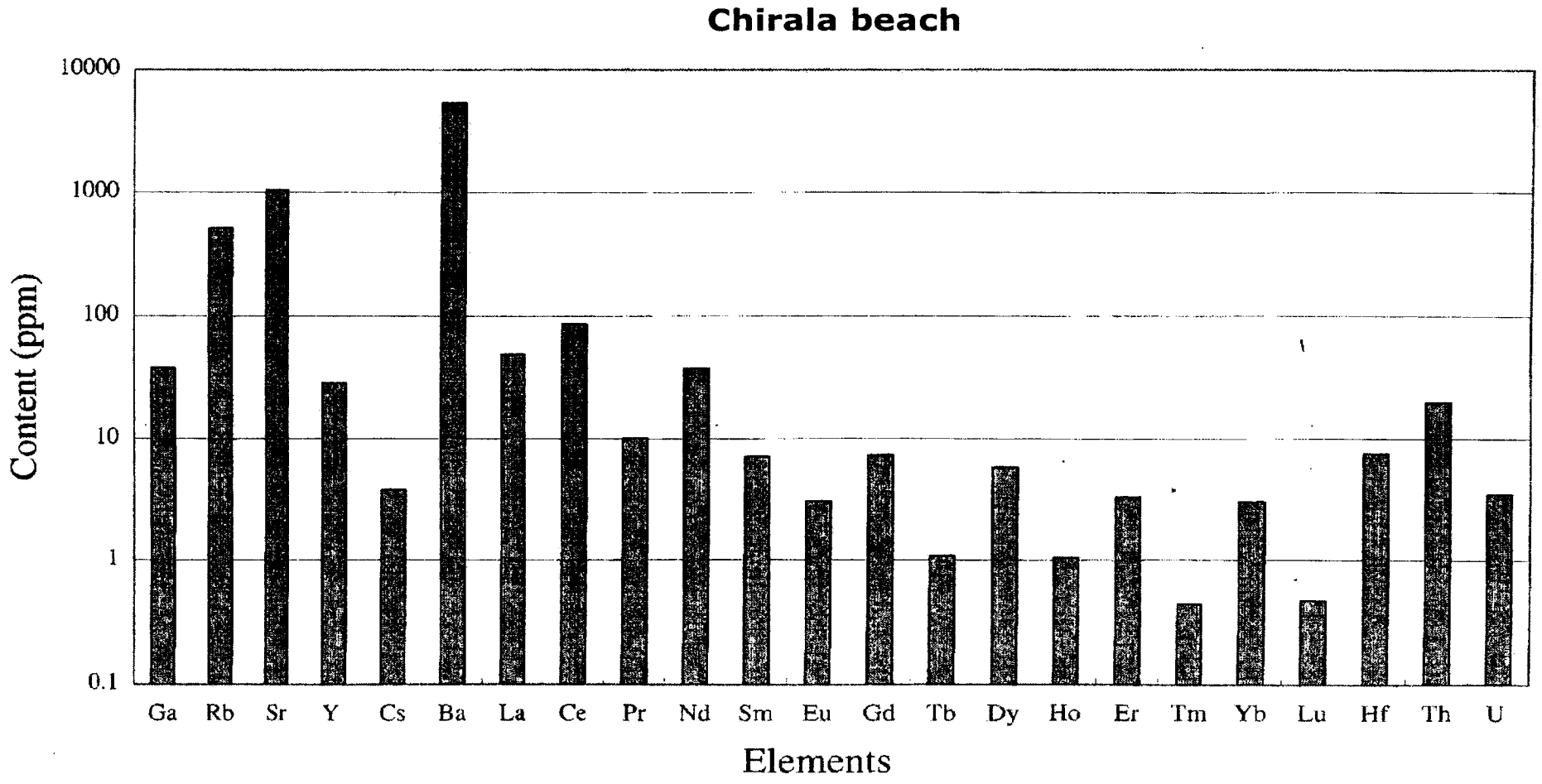

Fig 6.2 D: ICP-MS analysis
(Ga, Rb, Sr, Y, Cs, Ba, La, Ce, Pr, Nd, Sm, Eu, Gd, Tb, Dy, Ho, Er, Tm, Yb, Lu, Hf, Th, U)

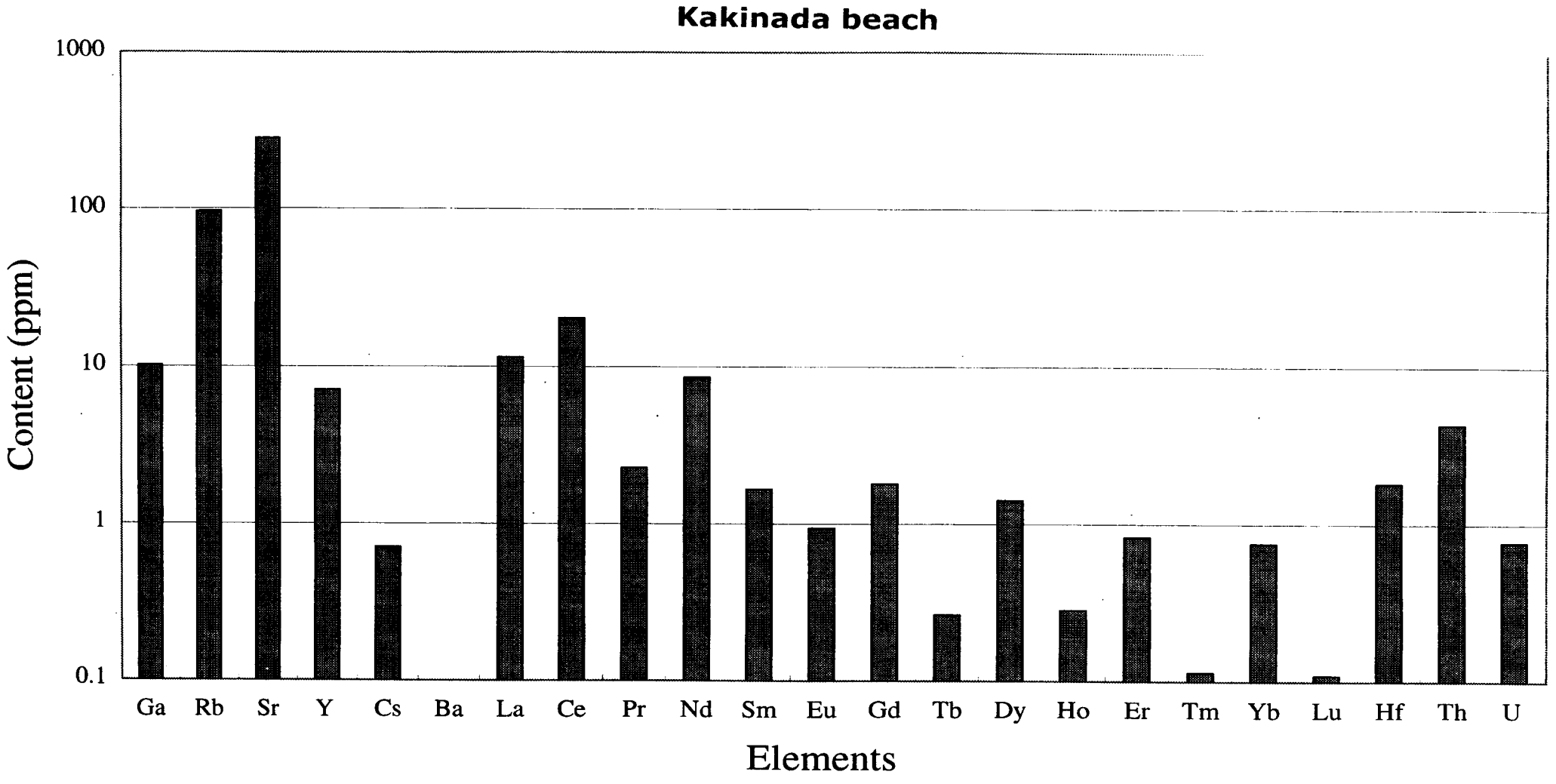

Fig 6.2 E: ICP-MS analysis

(Ga, Rb, Sr, Y, Cs, Ba, La, Ce, Pr, Nd, Sm, Eu, Gd, Tb, Dy, Ho, Er, Tm, Yb, Lu, Hf, Th, U)

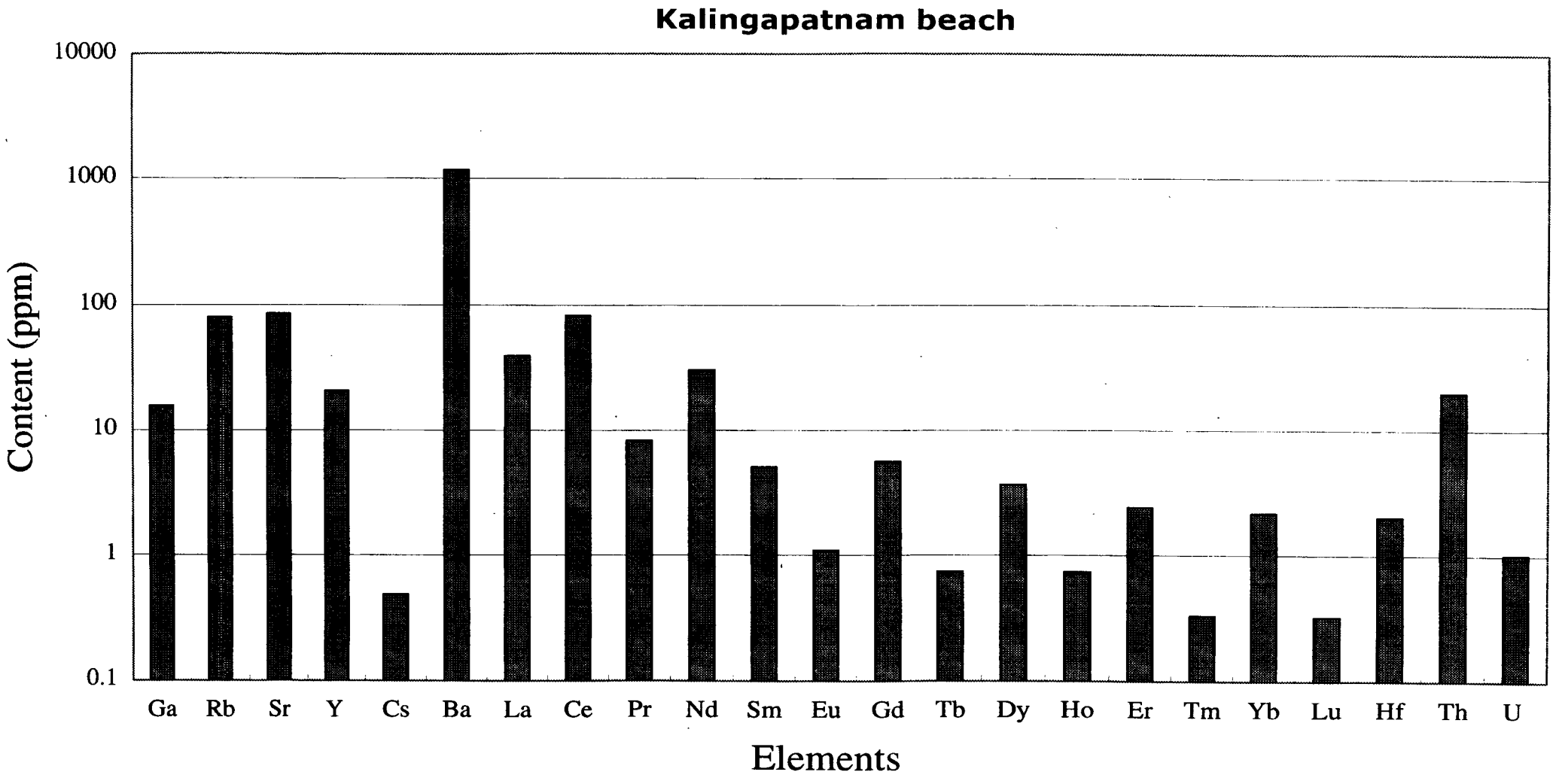

Fig 6.2 F: ICP-MS analysis

(Ga, Rb, Sr, Y, Cs, Ba, La, Ce, Pr, Nd, Sm, Eu, Gd, Tb, Dy, Ho, Er, Tm, Yb, Lu, Hf, Th, U)

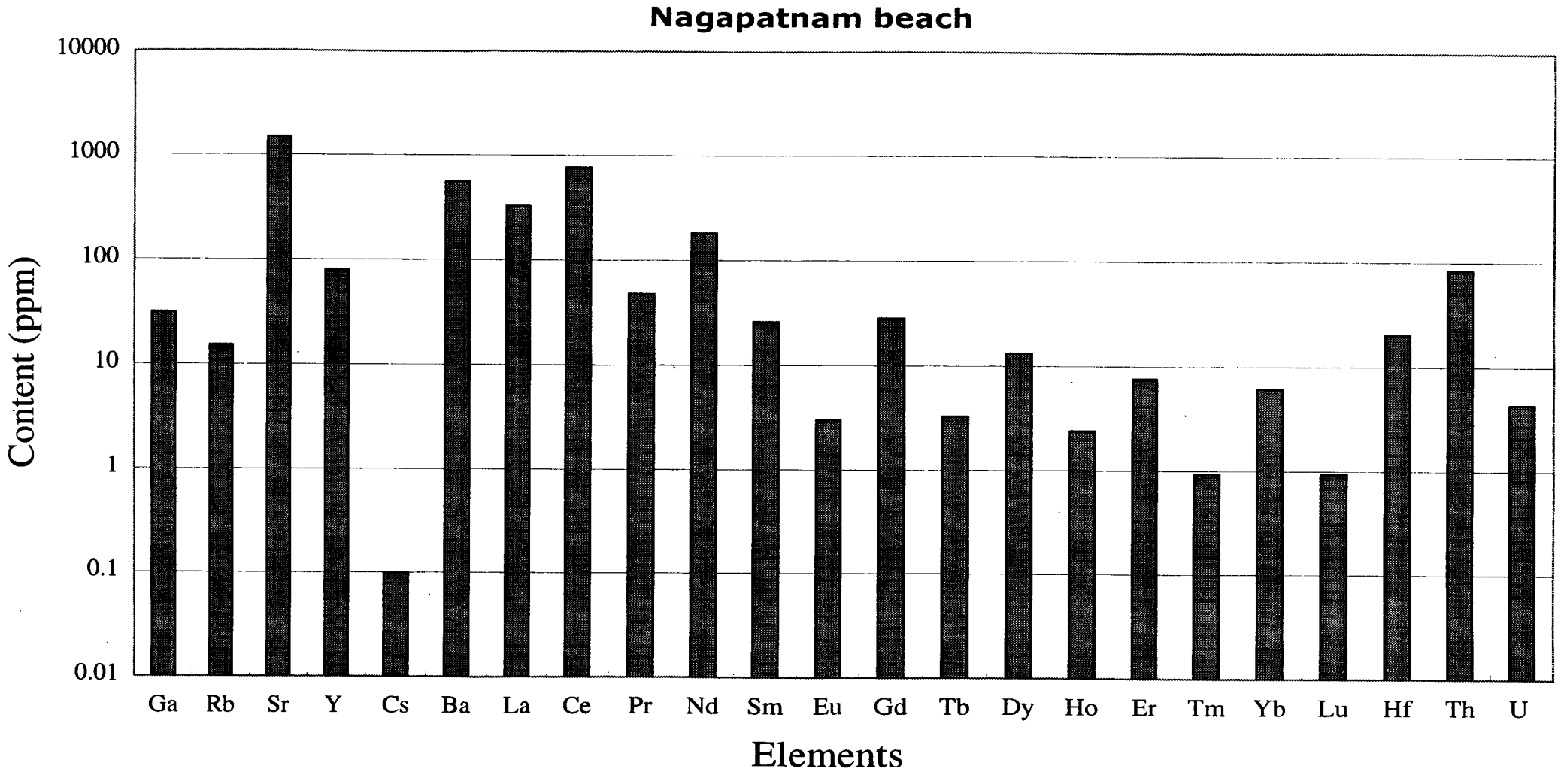

Fig 6.2 G: ICP-MS analysis

(Ga, Rb, Sr, Y, Cs, Ba, La, Ce, Pr, Nd, Sm, Eu, Gd, Tb, Dy, Ho, Er, Tm, Yb, Lu, Hf, Th, U)

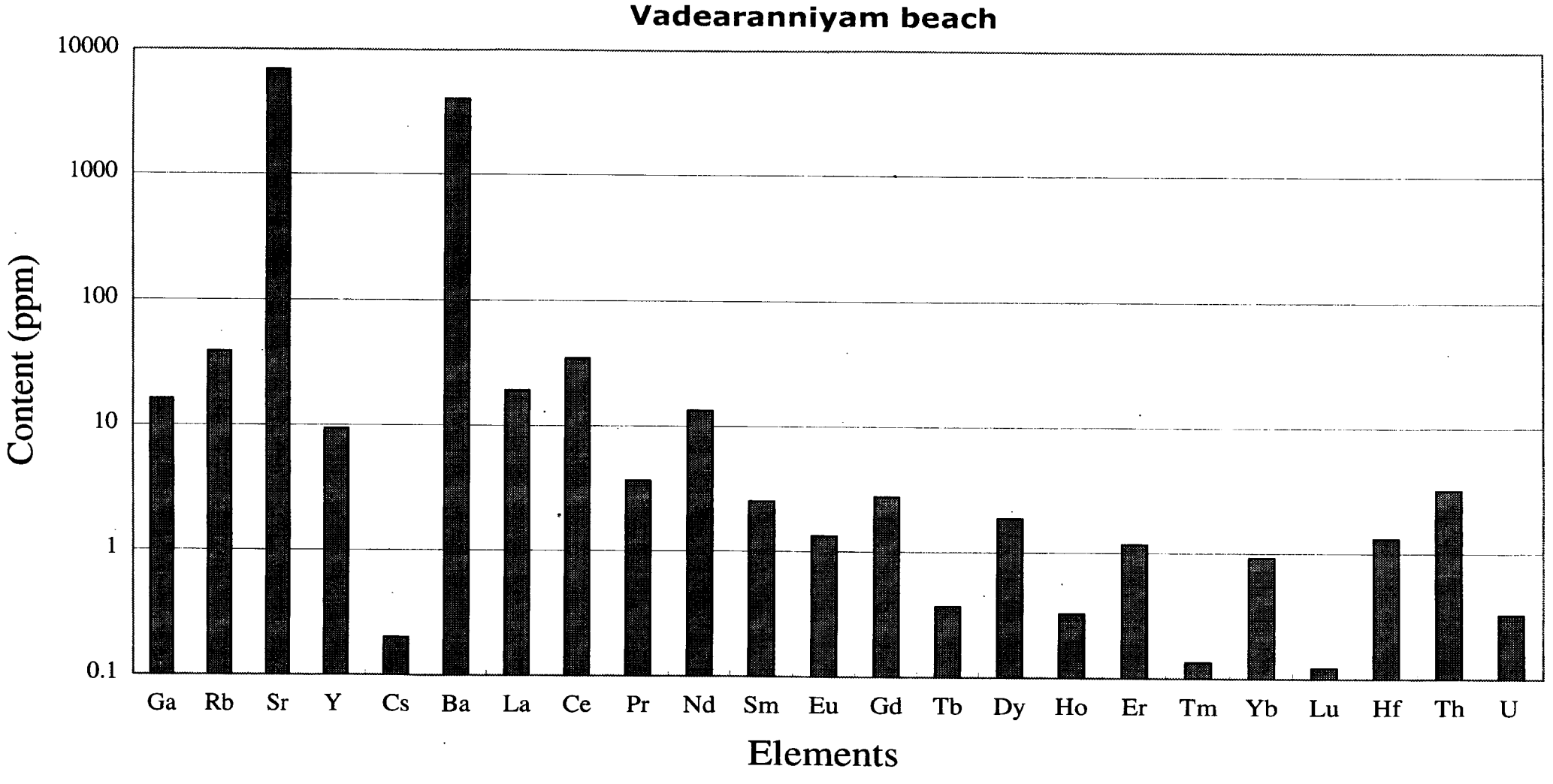

Fig 6.2 H: ICP-MS analysis

(Ga, Rb, Sr, Y, Cs, Ba, La, Ce, Pr, Nd, Sm, Eu, Gd, Tb, Dy, Ho, Er, Tm, Yb, Lu, Hf, Th, U)